Homology model directed alignment selection for comparative molecular field analysis: Application to photosystem II inhibitors

Mehran Jalaie* & Jon A. Erickson**
Dow AgroSciences, 9330 Zionsville Road, Indianapolis, IN 46268, U.S.A.

Summary

The use of a computational docking protocol in conjunction with a protein homology model to derive molecular alignments for Comparative Molecular Field Analysis (CoMFA) was examined. In particular, the DOCK program and a model of the herbicidal target site, photosystem II (PSII), was used to derive alignments for two PSII inhibitor training sets, a set of benzo- and napthoquinones and a set of butenanilides. The protein design software in the QUANTA molecular modeling package was used to develop a homology model of spinach PSII based on the reported amino acid sequence and the X-ray crystal structure of the purple bacterium reaction center. The model is very similar to other reported PSII protein homology models. DOCK was then used to derive alignments for CoMFA modeling by docking the inhibitors in the PSII binding pocket. The molecular alignments produced from docking yielded highly predictive CoMFA models. As a comparison, the more traditional atom-atom alignments of the same two training sets failed to produce predictive CoMFA models. The general utilities of this application for homology model refinement and as an alternative scoring method are discussed.

Introduction

Three Dimensional Quantitative Structure Activity Relationships (3D QSAR) are fast becoming standard tools in the area of drug and agrochemical design, especially in cases where the experimental structure of a ligand-receptor complex does not exist [1–5]. One of the most widely utilized 3D QSAR techniques is Comparative Molecular Field Analysis (CoMFA) [6] due to its success and wide range of applicability [5]. In the CoMFA formalism, the dependent variables are derived from potentials calculated between a probe atom at each vertex in a 3D grid of points and each atom of the 3D structures of a training set. A QSAR model is then derived from the variation in these calculated potentials and biological activity using the partial least squares (PLS) technique [7, 8]. It follows that CoMFA

models are directly dependent on the conformation and orientation of the molecules in the 3D grid, commonly known as the alignment rule. Not surprisingly, the key to derivation of a CoMFA model is molecular alignment.

Many approaches have been taken to address the alignment issue in CoMFA. Because correlation between interaction energies and binding affinity suggests information regarding the ligand-receptor complex, the ideal alignment would be provided by experimental structures of this complex [1, 2]. Unfortunately, the expense of having an experimental structure for every member of a training set is generally prohibitive. Furthermore, it is often the case that there is no experimental structure for even one representative ligand-receptor structure to use as a basis for an alignment scheme [9]. In the absence of any experimental structural data, several alignment strategies have been employed for CoMFA model development. The most common is based on a pharmacophore alignment where functional groups identified to be critical for binding are superimposed. Marshall's active analog

*Current address: Department of Chemistry, Indiana University-Purdue University at Indianapolis, Indianapolis, IN 46202, U.S.A.
**To whom correspondence should be addressed. Present address: Eli Lilly and Company, Lilly Corporate Center, Indianapolis, IN 46285, U.S.A.

method [10–12] for determining the binding conformation and functional group superposition has been used extensively with good success [1–5, 13]. Other pharmacophore methods have been applied to aligning molecules for CoMFA. For example, Martin et al.'s DISCO [14] method has been applied to neuromodulatory σ$_3$ receptor ligands to provide an alignment rule for a CoMFA model [15]. Another automatic pharmacophore method, CATALYST [16, 17], has been used to determine CoMFA molecular alignments for squalene epoxidase inhibitors [18] and obtusifoliol 14α-methyl demethylase inhibitors [19]. Others have used calculated fields to align molecules rather than pharmacophoric groups. For example, the field fit method within SYBYL [20, 21] was used to align cholescystokinin-A antagonists [22] and thermolysin inhibitors [23] to develop highly predictive CoMFA models. In addition, another field alignment algorithm, SEAL [24], has been used to align growth inhibitors of pancreatic tumors producing a useful CoMFA model [25].

In the absence of suitable pharmacophore information, many CoMFA studies rely on alignment of low energy conformations based on experimental or energy minimized structures of a congeneric training set [1, 2, 26–29]. The molecules are then aligned on common structural features. In these instances, CoMFA-derived fields do not represent the active site, but rather act as general shape descriptors in the QSAR. Based on these types of alignments, care must be taken regarding conclusions about the active site [1, 2].

The linkage of 3D QSAR and receptor information has been shown to be a powerful combination in bioactive design. Folkers et al. showed that CoMFA was useful in defining active site topologies which were very similar to independently derived protein models [29]. In fact, their work suggested that outliers in the CoMFA models may be due to different binding modes. The ability of CoMFA to provide qualitative receptor information was also shown in a study of phospholipase A2 inhibitors [30]. The use of structural information to guide alignment selection was used by Marshall and co-workers in studies on HIV-1 protease inhibitors to derive predictive CoMFA models [31]. In fact, they later developed a method to select among conformers for use in CoMFA by using minimizations within the active site [32]. Even the use of pseudoreceptors in combination with CoMFA has proved useful as the alignments for a CoMFA model of cannabinoids [33] were improved by using the pseudoreceptor software YAK [34] (now called PrGen [35]).

Although experimentally determined receptor-ligand structures are not often available, the information needed to construct 3D protein models from an amino acid sequence is becoming readily obtainable [36–38]. This data, along with a docking protocol, could be used to guide alignment selection for CoMFA. The strengths and weaknesses of the two methods are complementary. Knowledge-based protein models can provide 3D structural information that is critical for alignment in CoMFA, while the QSAR can provide better prediction of binding affinity than most methods for estimating binding energy, commonly known as scoring [39, 40]. Docking experiments have been used to validate alignments used in CoMFA. For example, the molecular alignments used for a CoMFA model of human rhinovirus inhibitors were supported by docking analogs into the crystal structure [41]. A similar validation was carried out for substrates of papain [42]. The use of a docking method applied to a homology model for the derivation of molecular alignments was pioneered by Rode et al. [43]. Because they were unable to correlate the estimated binding energies computed by AUTODOCK [44] of a highly diverse set of ligands to a model of monoclonal antibody, IgE(Lb4), they applied CoMFA. Using the alignments generated by AUTODOCK, highly predictive models were produced and were shown to be consistent with the binding site model.

In this report, the program DOCK [45–50] and a homology model of photosystem II (PSII) are used to produce molecular alignments for CoMFA. PSII has previously been the subject of several comparative modeling studies [51–59]. These are based on the X-ray crystal structure of the photosynthetic reaction center of the purple bacteria, *Rhodopseudomonas viridis* and *Rhodobacter sphaeroides* [60]. Analysis of the amino acid sequence homology between PSII from plant chloro and the *R. viridis* structure combined with mutagenesis and affinity labeling studies support the use of the bacterium structures as templates for model construction [51–59, 61]. PSII is composed of more than 20 polypeptide subunits, 2 of which, D1 and D2, form the heterodimer responsible for binding the redox components for the primary electron transfer. The D1 and D2 subunits in plant PSII are analogous to the L and M subunits of the purple bacterium structure, respectively. Inhibitors of PSII [62] disrupt electron flow in photosynthesis by competing with plastoquinone, an important electron acceptor, eventually stopping the production of ATP and resulting in cell death (see

Scheme 1). Therefore, PSII is the target of many widely used herbicides such as atrazine [63]. CoMFA has been applied to PSII inhibitors with some success. For example, a predictive CoMFA model was obtained for a set of anilide PSII inhibitors [64]. The first set of PSII inhibitors chosen for this study consists of benzo- and napthoquinones [65]. These inhibitors were selected to allow for direct comparisons of the docked structures to the orientation of plastoquinone in the model which is based on experimental data. The second set, butenanilides, was chosen for interest in the binding orientation from a design perspective [66].

Methods

Homology modeling

The basic steps in the construction of a protein model based on a homologous structure (i.e., an evolutionarily similar structure) are: amino acid sequence alignment, copying aligned coordinates, building loops, and finally refinement [36–38]. The Protein Design tools available in QUANTA [67] were used for all protein modeling.

The template structure chosen was the 2.3 Å resolution photosynthetic reaction center from *R. viridis* [60] available from the Brookhaven Protein Databank (PDB) as 1PRC. The unknown sequence was PSII from spinach [68]. The alignment suggested by Deisenhofer and Michel [61] was used to align the L and M subunits of the *R. viridis* reaction center with the D1 and D2 subunits of the spinach PSII, respectively. Each subunit was aligned and built separately and then combined for refinement.

After manually recreating the Deisenhofer and Michel alignment for the D1 subunit (see Figure 1), the coordinates of the homologous regions were copied from the L subunit of the *R. viridis* structure. In particular, the coordinates for residues 10–35, 38–71, 78–91, 93–96, 106–228, 234–241, 251–257, 260–264, and 266–314 were copied. Each of the regions was then regularized. Regularization is an energy minimization procedure used to clean up poor geometries but it ignores van der Waals terms. Regularization also builds coordinates for gaps of 3 amino acids or less. In order to build in the unknown structure for the 3 large gap regions (i.e., between 71 and 78, 96 and 106, 241 and 251), QUANTA's fragment searching function was utilized. This routine analyzes the inter-Cα distances of the residues in the search template (typically

Table 1. Fragments selected for gaps in D1

| Fragment	Protein	RMS difference (Å)
69–78	3rxn	1.072
95–108	3rxn	1.18
241–251	1rei	5.54

the 2 terminal residues on either side of the gap) to find a similar pattern in a database of protein structures. The fragments with the lowest root mean square (RMS) differences in inter Cα distances are located. The choice of a fragment to include in the model is based on the RMS difference, the fit with residues on either side, and the fewest number of close contacts to neighboring regions. Table 1 lists the fragments used to model the large gap regions in D1.

Using the Deisenhofer alignment did create a problem in the region close to the plastoquinone binding site and thus the alignment was altered slightly. In the Deisenhofer alignment, D1 has an insertion of F265 which is difficult to accommodate and still retain the hydrogen bond between S264 and the substrate. Because of the lack of homology other than the conserved serines (264 and 270) the insertion was changed to S268. In this position, there is a turn where the added amino acid does not significantly alter the binding region.

The residues 1–10 and 315–353 were removed as there were no coordinates to copy from the corresponding L structure and these regions were not close to the quinone binding site. Finally, the side chains were all examined for close contacts, and those found, relieved by the spinning protocol in QUANTA.

Even though the plastoquinone binding site is primarily in the D1 subunit, there are several regions of D2 that are very close to the binding site, necessitating the inclusion of D2 in the model. For the D2 subunit, the coordinates of the homologous regions were copied from the M subunit of the *R. viridis* structure again using the Deisenhofer–Michel alignment (see Figure 2). In particular, the coordinates for residues 1–25, 28–30, 32–36, 39–90, 92–95, 106–240, 250–256, 258–294 and 296–329 were copied. Each of these regions was then regularized to clean up poor geometries and to build in the coordinates for gaps of 3 amino acids or less. In order to build in the unknown structure for the 2 large gap regions (i.e., between 95 and 106, and between 240 and 250), QUANTA's fragment searching function was utilized. Table 2 lists the frag-
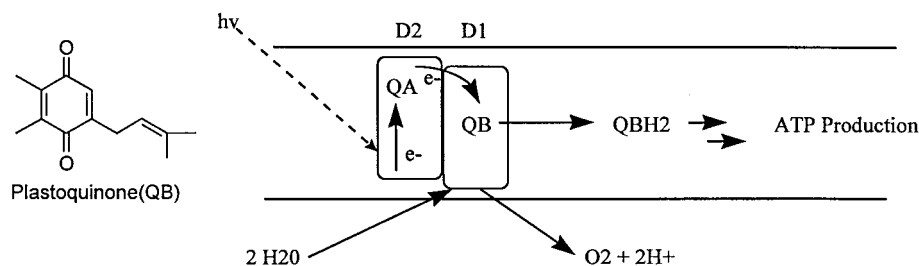
Scheme 1. Role of D1 and D2 subunits in photosynthesis. Light excitation of a chlorophyll in D2 causes a charge separation and an electron is passed to the first quinone (QA) from a pheophytin to form a semiquinone which subsequently reduces the second quinone (QB). This second transfer is inhibited by herbicides.

```
1prc_l          ---------ALLSFERKYRVRGGTLIGGDLFDFWV--GPYFVGFFGVSAIFFIFLGVSLI
d1              ---------SESLWGRFCNWITSTENRLYIGWFGVLMIPTLLTATSVFIIAFIAAPPVDI


1prc_l          GYAASQGPTWDP-------FAISINPPDLKYGL-GAAP----------LLEGGFWQAITV
d1              DGI-REPVSGS-LLYGNNIISGAIIPTSAAIGLHFYPIWEA-ASVDEWLYNGGPYELIVL


1prc_l          CALGAFISWMLREVEISRKLGIGWHVPLAFCVPIFMFCVLQVFRPLLLGSWGHAFPYGIL
d1              HFLLGVACYMGREWELSFRLGMRPWIAVAYSAPVAAATAVFLIYPIGQGSFSDGMPLGIS


1prc_l          SHLDWVNNFGYQYLNWHYNPGHMSSVSFLFVNAMALGLHGGLILSVANPGDG-------D
d1              GTFNFMIVFQAEH-NILMHPFHMLGVAGVFGGSLFSAMHGSLVTSSLIRETTENESA--N


1prc_l          KVKTAEH---------ENQYFRD--VVGYSIGA-LSIHRLGLFLASNIFLTGAFGTIASG
d1              EGYRFGQEEETYNIVAAHGYFGRLIFQYASFNNSRSLHFFLAAWPVVGIWFTALGISTMA
1prc_l_new                               S-IGALS


1prc_l          PFWTRGWPEWWGWWLDIPFWS
d1              FNLNGFNFN-QSVVDSQGRVI
```

Figure 1. Amino acid sequence alignment for *R. viridis* L and spinach D1 (see [60]). The modification made in alignment for the 264–270 region of D1 is shown (underlined).

```
1prc_m          ADYQTIYTQIQARGPHITVSGEWGDNDRVGKPFYSYWL--GKI-GDAQI--GPIYLGASG
d2              ------------MTIAVGKFTKD-EKDLFDSMDDWLRRDRFVFVGWSGLLLFPCAYFALG


1prc_m          IAAFAFGSTAILIILFNMAAEVHFDPLQFFRQFFWLGLYPPKAQYGM-GIPP--------
d2              GWFTGTTFVTSWYTHGLASSYLEGCNFLTAAVSTP----ANSLAHSLLLLWGPEAQGDFT


1prc_m          --LHDGGWWLMAGLFMTLSLGSWWIRVYSRARALGLGTHIAWNFAAAIFFVLCIGCIHPT
d2              RWCQLGGLWAFVALHGAFALIGFMLRQFELARSVQLRPYNAIAFSGPIAVFVSVFLIYPL


1prc_m          LVGSWSEGVPFGIWPHIDWLTAFSIRYGNFYYCPWHGFSIGFAYGCGLLFAAHGATILAV
d2              GQSGWFFAPSFGVAAIFRFILFFQGFH-NWTLNPFHMMGVAGVLGAALLCAIHGATVENT


1prc_m          ARFGGDREIEQITDRGTAVER---------AALFWRW-TIGFNATIESVHRWGWFFSLMV
d2              LF-EDGDGANT--FRAFNPTQAEETYSMVTANRFWSQIFGVAFSNKRWLHFFMLFVPVTG


1prc_m          MVSASVGILLTGTFV-DNWYLWCVKHGAAPDYPAYLPATPDPASLPGAPK
d2              LWMSALGVVGLALNLRAYDFVSQEIRAAEDPEFETFYTKNILLNEGIRAW
```

Figure 2. Amino acid sequence alignment for *R. viridis* M and spinach D2 (see [60]).

Table 2. Fragments selected for gaps in D1

Fragment	Protein	RMS difference (Å)
240–253	3cyt	1.62
94–108	3est	1.9312

ments used to model the large gap regions in D2. The amino acids without corresponding coordinates in M, 329-end, were deleted and close contacts found between the side chains were relieved using the spinning protocol in QUANTA.

The D1 and D2 subunits were merged based on the relative position of the L and M subunits from the *R. viridis* crystal structure. Ubiquinone from the *R. viridis* structure was mutated to plastoquinone and added to the structure for energy minimization. The CHARMm forcefield [69, 70] was used for all minimizations. The first minimization was performed on the model from the initial Deisenhofer–Michel alignment. In order to preserve the quinone binding site, D1 residues 198–292 and plastoquinone were fixed and 5000 steepest descent steps were performed. Subsequent to this, the D1 subunit was realigned as described above, and the coordinates for residues 260–267 were again copied from the L subunit and regularized. All but the active site residues (D1: 126–150, 209–239, 266–277 and D2: 1–42) were fixed and distance constraints were set in order to maintain the hydrogen bonds between plastoquinone and the protein. In particular, three constraints were defined, one between the quinone oxygen and the N-H of H215 and two between the other quinone oxygen and O-H of S264 and the backbone N-H of N266. These were set to be 2.1 Å with a minimum of 1.8 Å and a maximum of 2.7 Å and a penalty of 200 kcal mol^{-1}. The final model used for docking was similar to the X-ray structure. The Cα RMS deviation between D1 and L was only 0.80 Å and 1.15 Å between D2 and M.

Docking

The suite of docking software from the Kuntz group [71] was used to generate the docked alignments used in the CoMFA analysis. DOCK is a method of finding favorable orientations of ligands to a receptor. It works by filling the binding site of the receptor with spheres and then 'matching' the sphere centers to atoms of the ligands. These orientations are then evaluated with either a shape or binding energy scoring function fol-

lowed by a short minimization. There are several steps involved in using DOCK, including receptor preparation, sphere file generation, scoring grid generation and docking.

SYBYL [20] was used to prepare the PSII model for use with DOCK. In order to generate the sphere file, plastoquinone was separated from the PSII model. The DOCK utilities were used to extract a 10 Å sphere about plastoquinone from the model for use in sphere file generation. The generated sphere file was edited manually to include only spheres within the known binding region of the quinone (total of 36 spheres). For the energy scoring grid, hydrogens were added to all atoms of the PSII model and atomic charges (Kollman-all atom) were loaded. Ionization states were assigned assuming a pH of 7.0 so all arginines and lysines were assigned a net charge of 1.0 and all aspartates and glutamates were assigned a net charge of −1.0. Histidines were assumed to be neutral and the terminal amino acids were charged, yielding a total net charge of −5.0. The energy scoring grid was generated using a 6–12 potential function on a 14.294 Å × 18.256 Å × 16.445 Å grid with 0.3 Å spacing, a 10 Å non-bonded cutoff, the united atom model, and a distant dependent dielectric with a factor of 4.

Two sets of PSII inhibitors were docked into the model to obtain alignments for CoMFA analysis. The analogs were constructed using SYBYL, and CONCORD [72] was used to obtain low energy structures. SYBYL was used to add atomic charges using the Gasteiger method [73, 74]. In general, energy scoring was used with the grid previously described. The flexible 'anchor-search' method in DOCK was used to take ligand flexibility into account during docking while the protein remained rigid. In particular, 50 peripheral seeds were used in anchor search, 1000 orientations were obtained for each cycle and simplex minimization was performed with a convergence of 0.1 or 100 steps. In addition to the two training sets, Gasteiger charges were added to the structure of plastoquinone from the homology model and it was docked into the PSII model to examine the ability of DOCK to reproduce the model structure.

Comparative molecular field analysis

CoMFA, as implemented in SYBYL, was utilized in this work. For each of the training sets, two alignment strategies were examined. One alignment comes directly from the top scoring DOCK orientation, and the other relies on an atom based alignment. For the
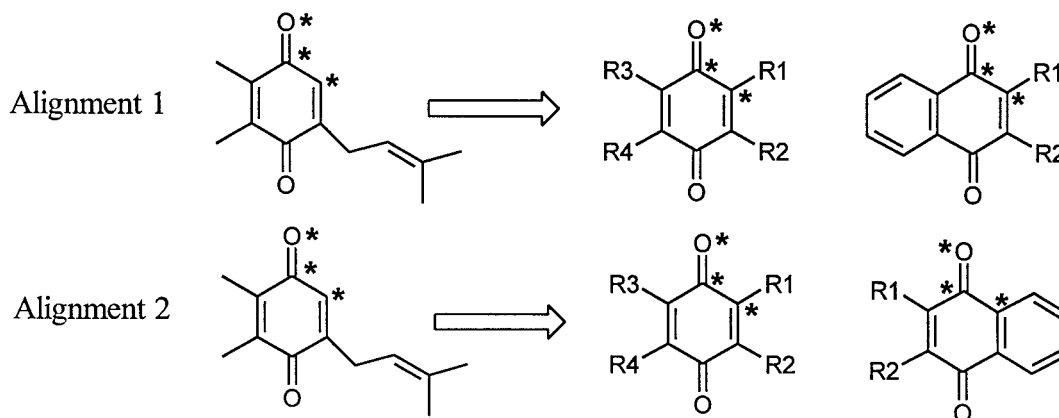
186

Figure 3. Atom based alignment of quinone training set (where R1 = small; R2 = large; R3 = R4 = similar size).

quinone training set, two atom based alignments were considered. Both of these can be described in relation to plastoquinone as shown in Figure 3. Basically these alignments differ with respect to overlay of the napthoquinones. In alignment 1, the phenyl ring overlays with the two methyl groups of plastoquinone and in alignment 2, the phenyl ring is aligned with the other side of the ring except in cases with a very large R2 substitutent. The analogs were overlaid by a least-squared fit on the 3 atoms marked with an *. DOCK could not find orientations for quinones 16 and 19, and thus these two analogs were not included in the CoMFA studies. For direct comparison to the docked based alignments, compounds 16 and 19 were also omitted from the atom-based models. The atom-based alignment for the butenanilide training set simply involved the overlay of the common structural features as the training set varies at only one position.

For each alignment in the two training sets, several CoMFA analyses were carried out in order to explore the effect of some of the CoMFA parameters. In particular, the sensitivity to position in the grid and grid spacing have been known to produce artifacts [75, 76]. The effect of grid spacing was probed by deriving CoMFA models using 1 Å and 2 Å grids. Specifically, the grid dimensions for the quinone set were 18 Å × 22 Å × 18 Å, yielding 1200 points at a 2 Å resolution and 8303 points at 1 Å. For the butenanilides, 16 Å × 20 Å × 18 Å grids with 990 and 6783 points and at 2 Å and 1 Å, respectively, were used. In addition, the position of the analogs inside the grid was explored by rotating the molecules in the lattice. A slightly different grid was used for this experiment as the molecules were first centered (removing the molecules from the coordinate space of the protein) and then rotated. This grid was 20 Å × 12 Å × 12 Å with 3549 points for the quinones and 20 Å × 12 Å × 14 Å with 4095 point for the butenanilides. For comparison to the traditional QSAR's, steric only fields were calculated in addition to the default combined steric and electrostatic fields. All of the other CoMFA parameters used were the SYBYL default values. A sp^3 C^+ probe, distance dependent dielectric and 30 kcal mol^{-1} cutoff were used in the field calculation. Cross-validated (leave-one-out protocol) PLS analyses were carried out to identify the optimal number of components (i.e., latent variables) yielding the highest cross-validated r^2 (q^2) and the lowest standard error of prediction using the SAMPLS method [77]. Non-crossvalidated PLS analyses were carried out at the optimal number of components using the default convergent criteria (0.0001 with 100 maximum iterations) and standard scaling. The IVS-PLS region focusing method of Wold et al. [78] was subsequently applied to the optimal models as it has shown the ability to improve predictability and was available within SYBYL. The dependent variable for the quinone set was the $\log(1/I_{50})$ or pI_{50} where I_{50} is the concentration to inhibit photosynthetic electron flow from water to DCPIP to 50% in green algae cell free thylakoid membranes [65]. For the butenanilides, the biological activity used for the dependent variable was the percent [14C]-atrazine displacement in spinach thylakoid membranes at a 10 μM concentration of inhibitor [65]. The standard deviation * coefficient CoMFA maps were plotted at the 80% and 20% contribution levels representing both high (where steric bulk/positive charge increase activity) and low values (where steric bulk/positive charge decrease activity), respectively.

Figure 4. Overlay of the Cα trace of the D1 and D2 subunits of spinach PSII homology model (black) and the L and M subunits of *R. viridis* reaction center X-ray crystal structure (gray).

Results and discussion

Homology modeling

The spinach PSII homology model is shown in Figure 4, overlaid with the crystal structure of the purple bacterium structure. Overall, the model is very similar to those produced in earlier studies. The active site, shown in Figure 5, shows a slight shift in the position of the quinone relative to that in the *R. viridis* structure. The hydrogen bonds from the quinone to H215 and F265 retain the same length, but that to S264 is lengthened as was seen in previous models [55]. This is consistent with mutagenesis experiments where quinone-type inhibitors retain activity when S264 is mutated to an alanine [65].

Docking

The first docking experiment was performed in order to reproduce the modeled orientation of plastoquinone in the PSII model with DOCK. Table 3 shows the

Table 3. Docking results of plastoquinone to PSII model

Orientation	Score
1	−29.90
2	−29.75
3	−29.53
4	−29.23
5	−28.82
6	−28.55
7	−28.37
8	−28.02
9	−27.98
10	−27.86

scores of the top 10 orientations. The first two orientations fit very closely to the modeled structure. The quinone head is shifted slightly in both and the two orientations differ with respect to each other only in
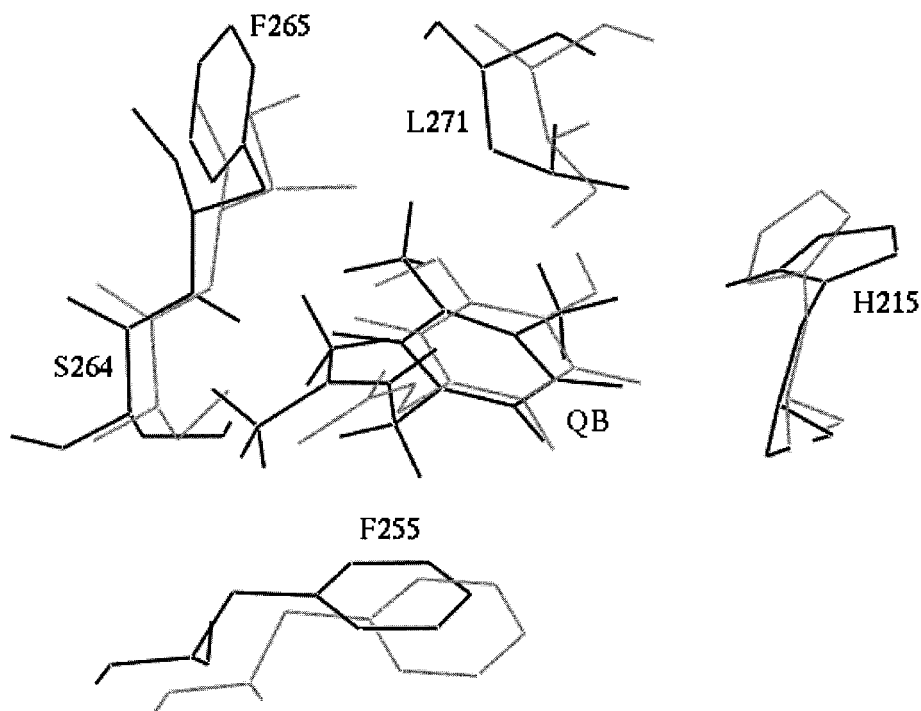
Figure 5. Quinone binding sites of the spinach PSII homology (black) model and *R. viridis* X-ray crystal structure (gray) overlaid. (Amino acids for PSII model are indicated.)

the conformation of the prenyl group as shown in Figure 6. The ability of DOCK to predict the binding of the substrate into the model gave us the confidence to use it for docking inhibitors.

The results of docking the quinone training set to the PSII model are shown in Table 4. Only the score for the top scoring orientation for each molecule is indicated, even though the top fifty scoring orientations were examined. Comparison of the benzoquinone inhibitors (12–23) shows a fairly close fit with the modeled orientation of plastoquinone with the exception of compounds 16 and 19. None of the top fifty orientations produced by DOCK were able to place these two large analogs into the binding pocket. This may point to areas in the homology model that need refinement and the problems with using a rigid active site for docking. The top scoring orientations for the napthoquinones, however, did not mirror that of the modeled quinone. The orientations of the napthoquinones were rotated such that the 4-position corresponds to the 3-position of plastoquinone. In this orientation, the hydrogen bond to H215 is lost, but the other two are maintained. Although the orientations of the quinones produced by DOCK were promising, the scores did not correlate at all with activity as shown in

Figure 7. Because of the known problems with scoring (i.e., lack of solvation, neglect of entropy, rigid protein etc.) and the use of activity data from another species (green algae and not spinach), a perfect correlation was not expected, however, some sort of trend would be necessary if docking alone was used to understand and predict relative binding affinity.

The results of the docking experiments for the butenanilides are shown in Table 5. The top scoring orientations for each were very similar, placing the chlorophenyl group over the quinone ring and the rest of the structure projecting into the same pocket as the prenyl group of plastoquinone. In four of the analogs (see Table 5) the top scoring orientation did not exhibit the same general alignment as the other thirteen, however, in each case, a top scoring orientation did conform to the general alignment of the majority and thus were used in the CoMFA model. As in the case of the quinones, no correlation between DOCK scores and activity was found as shown in Figure 8.

Comparative molecular field analysis

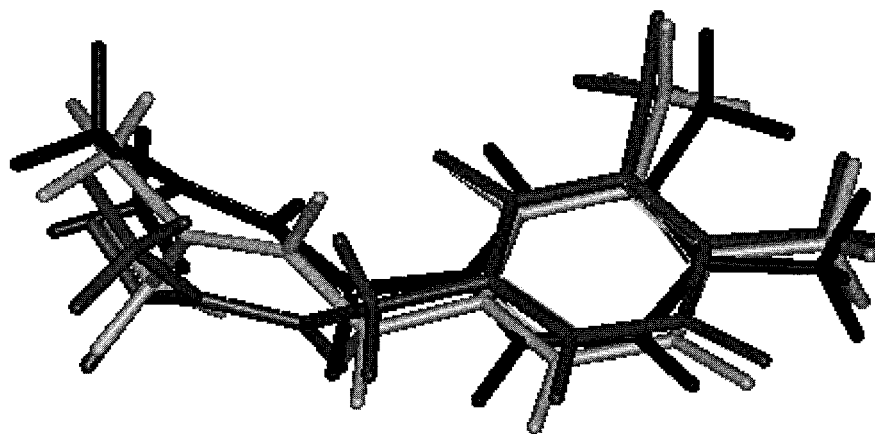Table 6 shows the comparison between the quinone CoMFA models derived from the two atom-based

Figure 6. Top 2 DOCK orientations (#1 dark gray, #2 light gray) of plastoquinone compared to the modeled structure (black).
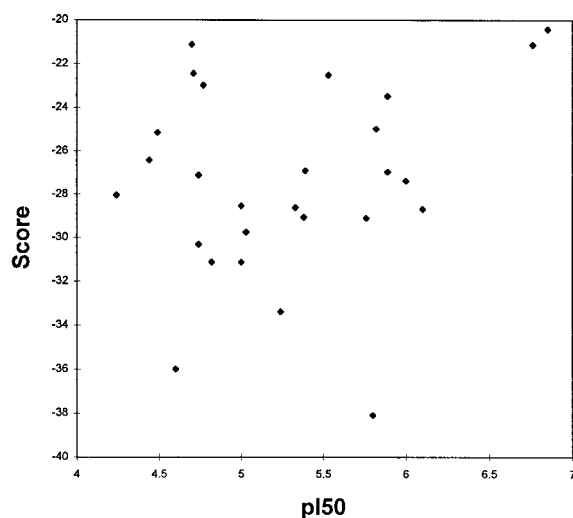

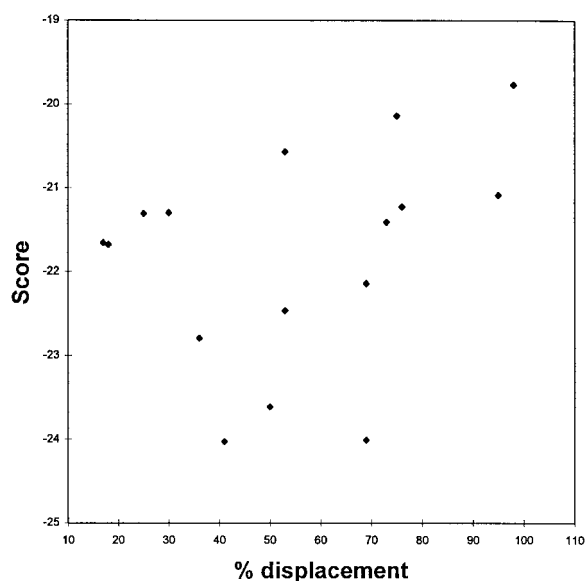*Figure 7.* Activity vs. DOCK score for the quinone training set.

Figure 8. Activity vs. DOCK score for the butenanilide training set.

alignments and those from the docked alignments (see Figure 9). Examination of the q^2's of the models shows that predictive models could not be found for the atom-based alignments using either an electrostatic and steric field in combination or with a steric field alone for the full quinone data set. This result was initially surprising due to the previously found correlations with steric descriptors. Because Draber et al. [65] found classical QSAR models using STERIMOL [79] shape parameters to explain the same bioactivity data for the benzoquinone and napthoquinone series separately, CoMFA models were run for both atom-based alignments for each series. Table 6 shows that CoMFA models of predictive ability ($q^2 \sim 0.5$) can be found using alignment 1 and the steric fields only for both classes of quinones, consistent with the previ-

ous QSAR models. In this instance, the CoMFA fields are acting only as general steric descriptors and do not necessarily describe the binding pocket. When the two sets are combined without knowing their relative binding orientations, the ability of the CoMFA fields to act as general steric descriptors breaks down.

The alignments from docking the quinones into the PSII homology model, however, produce a predictive 3-component CoMFA model for the combined set of benzo- and napthoquinones, with a q^2 of ~0.5 using the standard grid spacing. These results show that the relative orientations of the benzo- and napthoquinones from DOCK produce variation in the steric and electrostatic fields that correlate with experimental binding
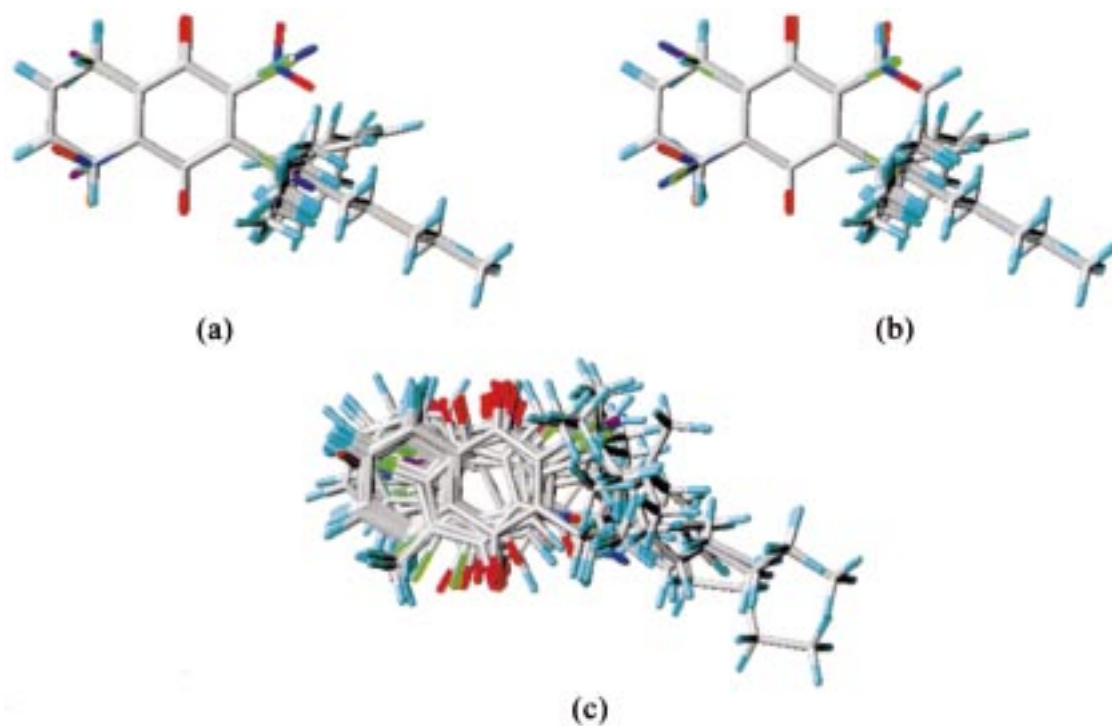
Figure 9. CoMFA alignments of the quinone training set. (a) Atom-based alignment 1. (b) Atom-based alignment 2. (c) Dock-based alignment.
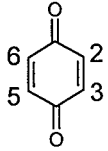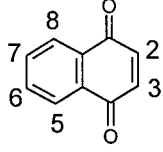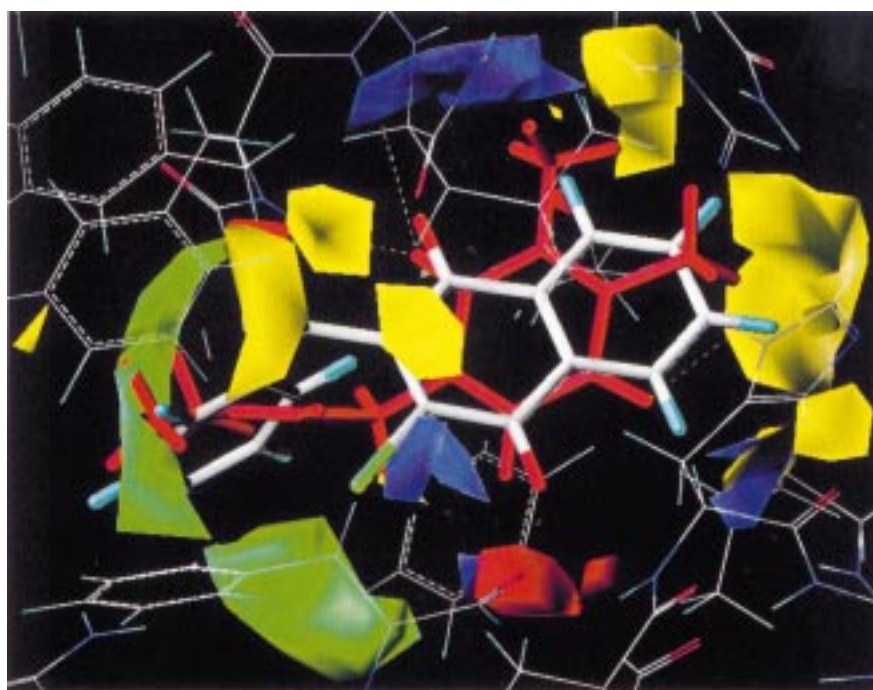

Figure 10. Steric (green = 80% contribution; yellow = 20% contribution) and electrostatic (blue = 80% contribution; red = 20% contribution) CoMFA coefficient maps of the quinone training set superimposed on the PSII model. Plastoquinone (red) from the model and the DOCK alignment of analog 32 (atom colors) are shown.

Table 4. Dock results and activity of quinone training set

Molecule		pI_{50}	Score
12	2,5,6-Br$_3$,3-Me	4.44	-26.42
13	2,3-Cl$_2$,5-CMe$_3$	4.49	-25.15
14	2,5-Br$_2$,3-Me,6-CHMe$_2$	4.70	-21.11
15	2,3,5,6-Cl$_4$	4.74	-27.11
16	2,5-Br$_2$,3,6-(OCHMe$_2$)$_2$	4.77	-22.97
17	2,3-Br$_2$,5-CMe$_3$	5.53	-22.50
18	2,3,5,6-Br$_4$	5.82	-24.97
19	2,3,5,6-I$_4$	6.76	-21.13
20	2,3-I$_2$,5-CMe$_3$	6.85	-20.42
21	2,5-(NO$_2$)$_2$,3-Me,6-CHMe$_2$	4.71	-22.43*
22	2,5,6-Br$_3$,3-(CH$_2$)$_5$Me	5.24	-33.38
23	2-CMe$_3$,5,6-Br$_2$	5.89	-23.47

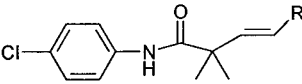| Molecule		pI_{50}	Score
24	2Br	4.24	-28.04
25	2-Cl,3-Me	5.00	-28.53
26	2-CH$_2$Cl,3-Cl	5.00	-31.13
27	2,3-Cl$_2$	5.33	-28.60
28	2-Br,3-Me	5.38	-29.05
29	2,3-Br$_2$	5.76	-29.09
30	2-Br,3-(CH$_2$)$_6$Me	5.80	-38.10
31	2-Br,3-CHMe$_2$	5.89	-26.96
32	2-Br,3-CH$_2$Ph	6.00	-27.37
33	2,3-I$_2$	6.10	-28.68
34	2-(CH$_2$)$_3$Me	4.74	-30.32
35	2-CH$_2$Ph	4.82	-31.12
36	2-(CH$_2$)$_6$Me	4.60	-35.98
37	2,3-(CN)$_2$	5.03	-29.75
38	2-CHMe$_2$,3-Br	5.39	-26.90

* The orientation for 21 used for the CoMFA analysis was not the top scoring, but #3 in rank. The top score for this molecule was -23.64.

affinity. This suggests that, although the raw scores produced by DOCK do not correlate with I$_{50}$s, the relative orientations of the inhibitors in the binding pocket are predicted. No surprises were found for the benzoquinones as they align in a similar fashion to the modeled substrate, but the combined DOCK and CoMFA results predict a non-intuitive alignment for the napthoquinones.

In order to further analyze the CoMFA results of the docked alignment, some of the CoMFA parameters were examined. One potential source of error in CoMFA is the position of the molecules in the lattice [1]. Changing the distance between a molecule and

Table 5. Dock results and activity of butenanilide training set

Molecule	R	%[^{14}C]Atrazine displacement	Top Score*
LY808214	Me	25	-21.31
LY219451	CN	53	-23.62 (#5,-22.46)
LY221204	Cl	17	-21.66
LY215157	CCH	76	-22.55 (#6,-21.23)
LY210835	SO$_2$Me	73	-22.55 (#2,-21.41)
LY272045	NO$_2$	69	-22.14
LY210834	SOMe	95	-21.09
LY277088	F	41	-24.03
LY209209	H	75	-20.14
LY210837	SPh	69	-24.01
LY233695	CF$_3$	53	-20.57
LY257264	Br	18	-21.68
LY232969	SMe	36	-22.79
LY207283	Ph	98	-21.86 (#4,-19.77)
LY233548	OMe	50	-23.61
LY222238	I	30	-21.30
LY274542	OC(O)Me	95	-25.67

*The top scoring orientation was not used in the CoMFA modeling for these analogs.
The rank and score of the orientation used is given in parentheses.

a grid point can drastically change the potential calculated, especially for a steep function like that used for the steric field. In order to explore this dependence, two additional CoMFAs were performed (see Table 6). In the first, the grid spacing was simply decreased from 2 Å to 1 Å, which should lessen the chance of a grid position artifact. In this case, the q^2 remained fairly constant. A second method of detecting grid position dependence involves rotation of the molecules in the lattice, keeping the same positions of the molecules relative to each other. The original grid was created in the coordinate space of the PSII model; for ease of manipulation, the set was centered to create the original and rotated sets for comparison. The rotated set was manually rotated about 45° about the x-axis. A new region file was created which enclosed both training sets. Cross-validated SAMPLS analysis on both sets revealed only a small difference in q^2.

The region focusing [76] method was used to refine the final model to generate contour coefficient maps for comparison to the PSII model. The region focusing method implemented in SYBYL was used to increase the q^2 of the model as shown in Table 6. In order to

further demonstrate the predictive ability of the model beyond cross-validation, a test set was extracted from the training set, a CoMFA model derived, and the test set predicted. Five analogs were chosen by sorting the training set according to pI$_{50}$ and selecting every fifth compound, producing a test set including analogs 21, 23, 24, 25 and 38. Thus compounds were selected which span a range in activity and structure (2 benzoquinones and 3 napthoquinones). Using a 1 Å grid and the new region-focused lattice, cross-validated SAMPLS revealed an optimum q^2 of 0.5 at 2 components. The 2-component CoMFA model ($r^2 = 0.863$; Standard Error of Estimate (SEE) = 0.253) was then used to predict the activity of the test set, revealing a fairly predictive model with an actual vs. predicted r^2 of 0.78 (see Table 7). In addition, both the 20- and 25-compound models exhibited very similar CoMFA coefficient maps.

The CoMFA coefficient maps of the final region-focused model (PLS at 3 components: $r^2 = 0.892$; SEE = 0.224) are displayed in Figure 10 superimposed on the PSII model including plastoquinone and one of the napthoquinones (molecule 32). The steric

Table 6. CoMFA results for quinone training set

Description	Alignment	n	Grid (Å)	Field	# Comp.	q^2
All	Atom-1	25	2	Both	5	−0.266
All	Atom-1	25	2	Steric	5	−0.125
All	Atom-1	25	1	Both	5	−0.129
All	Atom-1	25	1	Steric	5	0.251
All	Atom-2	25	2	Both	3	−0.402
All	Atom-2	25	2	Steric	4	−0.186
All	Atom-2	25	1	Both	5	0.000
All	Atom-2	25	1	Steric	5	0.069
benzoquinone	Atom-1	10	1	Steric	4	0.457
benzoquinone	Atom-2	10	1	Steric	4	0.449
napthoquinone	Atom-1	15	1	Steric	5	0.580
napthoquinone	Atom-2	15	1	Steric	4	0.119
All	Docked	25	2	Both	3	0.497
All	Docked	25	1	Both	2	0.438
All (centered)	Docked	25	1	Both	2	0.454
All (rotated)	Docked	25	1	Both	2	0.438
All (region focused)	Docked	25	1	Both	3	0.619
Test (All less 5)	Docked	20	1	Both	2	0.505

Table 7. Predicted activities for the quinone test set

Molecule	Actual pI_{50}	Predicted pI_{50}
24	4.24	4.51
21	4.71	4.57
25	5.00	5.18
38	5.39	5.59
23	5.89	5.44

maps coincide with the PSII model, showing green contours, where steric bulk increases activity, in open regions in the active site such as the channel where the prenyl group of plastoquinone lies (above F255 and between F265 and F211). The yellow regions correspond to the areas where steric bulk decreases activity and the overlay with the protein model indicates they align with the sides of the binding pocket (L271, V219 and the backbone of N267). In contrast to the steric coefficient maps, the electrostatic maps contain some inconsistencies. For example, there is a blue contour (positive charge increases activity) in the region where there is a putative hydrogen bond between the plastoquinone carbonyl oxygen and H215 in the binding pocket. This can be attributed to the alignment of the napthoquinones that places the carbonyl group in a different region of space. This result could point to areas where the homology model could be refined, for example allowing H215 to be flexible to move closer to the adjacent red region (where negative charge increases activity). The other two blue regions correspond to relatively hydrophobic regions (V219 and F211) which could accommodate non-polar groups.

Table 8 displays the results for the CoMFA analyses of the butenanilide series. The atom-based alignment failed to produce a predictive CoMFA ($q^2 = 0.129$) using the steric and electrostatic fields in combination. The model improved slightly ($q^2 = 0.211$) when only the steric fields were considered, as was the case with the quinone set. This is not surprising given the correlation found between this same training set and STERIMOL shape descriptors [65]. Again, for a series of congeners, CoMFA fields can act as general shape descriptors.

The docked alignments for the butenanilides do not differ radically from the atom-based alignments as shown in Figure 11. For each analog, the p-chlorphenyl, amide and R groups occupy a very similar area of space, but are not aligned atom to atom. This may reflect a more realistic binding orientation

Table 8. CoMFA results for the butenanilide training set

| Description	Alignment	n	Grid (Å)	Field	# Comp.	q^2
All	Atom	17	2	Both	1	0.053
All	Atom	17	2	Steric	2	0.131
All	Atom	17	1	Both	2	0.129
All	Atom	17	1	Steric	2	0.211
All	Dock	17	2	Both	2	0.308
All	Dock	17	2	Steric	3	0.591
All	Dock	17	1	Both	1	0.209
All	Dock	17	1	Steric	2	0.421
All (centered)	Dock	17	1	Steric	2	0.384
All (rotated)	Dock	17	1	Steric	2	0.376
All (region focused)	Dock	17	1	Steric	2	0.571
Test (all less 3)	Dock	14	1	Steric	2	0.464
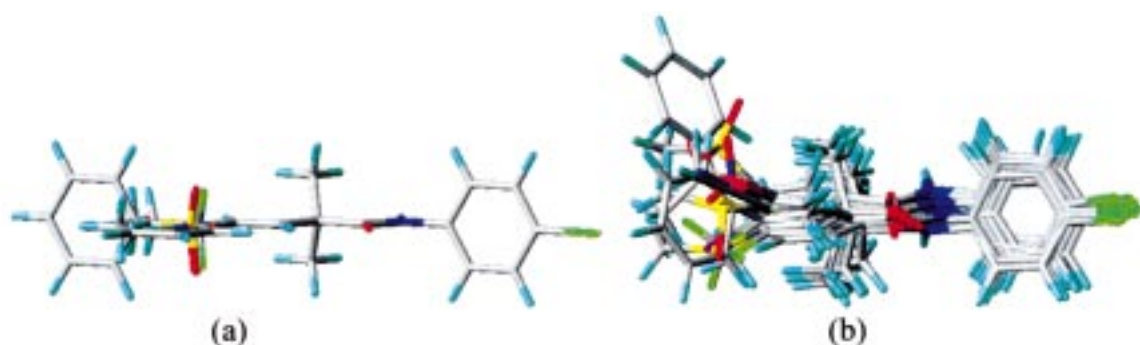
Figure 11. CoMFA alignments for the butenanilides. (a) Atom-based alignment. (b) Dock-based alignment.

given the perturbation created by changes in size of the R group in a binding pocket that does not change much in the interaction. This claim is supported by the improvement in predictability that the docked alignment model provides over the atom-based model as shown in Table 8. For both, the combination field and the steric alone field, q^2 are higher for the dock alignment models. Unlike the quinone set, the docked alignments of the butenanilides seem to be less invariant to smaller lattice spacing, however, the q^2 differences are small with respect to rotation within the grid. For this reason, the 1 Å grid models were used.

The final butenanilide model was derived using the steric only field and the region-focusing method in SYBYL to produce a 2-component model with a $r^2 = 0.869$ and a SEE = 10.292. A test set was taken from the original 17 in order to more fully examine the predictability of the model. The test set was chosen in a similar manner to that used with the quinone set, the analogs were sorted according to activity and

Table 9. Predicted activities for the butenanilide test set

Molecule	Actual % displacement	Predicted % displacement
LY232969	36	48
LY210837	69	71
LY210834	95	86

three compounds were selected to span activity and structural variation. The model was then derived again using the 14 remaining analogs. A model with an optimum of 2 components ($q^2 = 0.464$) was found by performing cross-validated PLS using the region focused lattice. The 2-component model (PLS $r^2 = 0.879$; SEE = 10.158) was then used to predict activities of the 3 members of the test set. The predicted vs. actual r^2 of 0.99 revealed the predictability of the model (see Table 9).
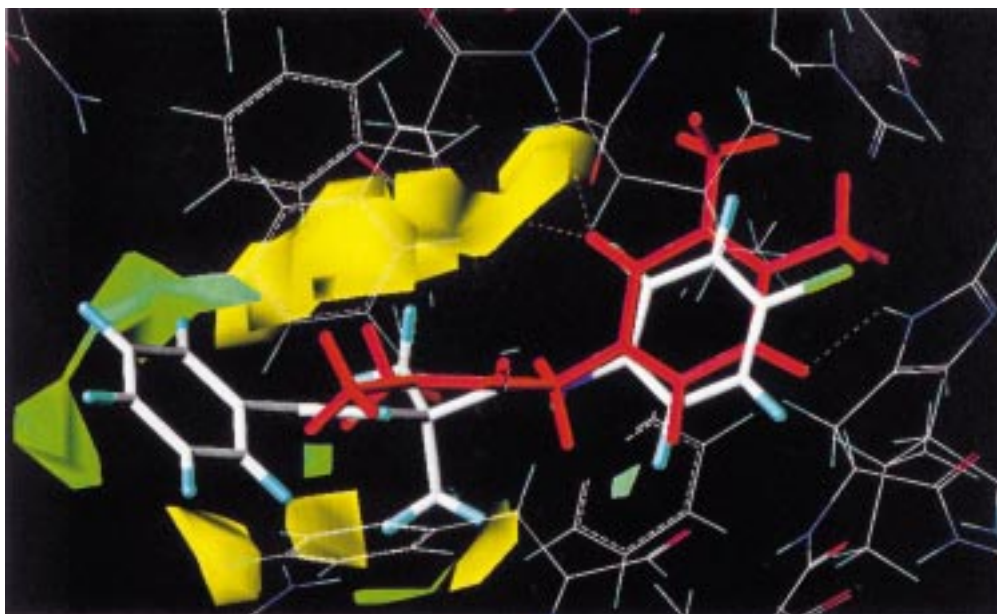
Figure 12. Steric (green = 80% contribution; yellow = 20% contribution) CoMFA coefficient maps of the butenanilide training set superimposed on the PSII model. Plastoquinone (red) from the model and the DOCK alignment of LY207283 (atom colors) are shown.

The CoMFA coefficient maps (shown in Figure 12) are very consistent with the binding pocket of the PSII homology model. The maps highlight the variation in the series showing a sterically favorable area (in green) at the end of the groove where the prenyl group of plastoquinone lies. Sterically unfavorable regions (in yellow) align with the sides of this groove in the binding site model.

Conclusions

The use of 3D QSAR and protein homology modeling together is a powerful combination for bioactive design since both methods complement the other's weakness. Bioactive conformations and alignments, the critical information required by CoMFA, can be obtained using a docking protocol and a homology model in the absence of an experimental structure of the receptor-ligand complex. In the case of the quinone PSII inhibitors, the alignments provided by using DOCK and the homology model were critical in obtaining a 3D QSAR model. Without this information, the CoMFA fields act only as general shape descriptors, and not as a reflection of the binding site. Even for the butenanilide training set, the variation in the steric fields produced by the docked alignments gave more predictive CoMFA models. This result highlights

the observation that structural perturbations, even in one position, have the ability to alter binding suggesting that atom-to-atom superpositions in 3D QSAR may not be realistic.

3D QSAR complements docking algorithms because the predictive model can be used in place of the scoring functions of most docking methods to help prioritize targets. Scoring functions often perform poorly due to neglect of such important factors to binding energies as solvation and entropy. These shortcomings can be overcome with the use of a training set and a regression method. For both the quinones and butenanilides, the scoring function was unable to rank inhibitors. On the other hand, the orientations from DOCK did correlate with variation in their steric and electrostatic fields in the CoMFA models, indicating that the predicted binding modes may have merit.

In addition, the 3D QSAR model can help in refining the protein model. In this study, one region of the electrostatic CoMFA coefficient map is inconsistent with the protein model. This information could be used, for example, to refine the model by side-chain rotation. The 3D QSAR models were also useful in identifying an alternative binding mode of the napthoquinones in this study. The ability to produce predictive CoMFA models using the orientations from DOCK where the more 'intuitive' atom-based alignments failed, suggests an alternative binding mode for

the napthoquinones. In general, the added ability to correlate the modeled protein structure with experimental binding affinities provides another method to support the accuracy of the model.

References

1. Cramer, R.D. III, DePriest, S.A., Patterson, D.E. and Hecht, P., In Kubinyi, H. (Ed.), 3D QSAR Drug Design: Theory, Methods and Applications, ESCOM, Leiden, 1993, pp. 443–485.
2. Folkers, G., Merz, A. and Rognan, D., In Kubinyi, H. (Ed.), 3D QSAR in Drug Design: Theory, Methods and Applications, ESCOM, Leiden, 1993, pp. 583–618.
3. Hopfinger, A.J. and Tokarski, J.S., In Charifson, P.S. (Ed.), Pract. Appl. Comput.-Aided Drug Des., Dekker, New York, NY, 1997, pp. 105–164.
4. Martin, Y.C., Kim, K-H. and Lin, C.T., Adv. Quart. Struct.-Prop. Relat., 1 (1996) 1.
5. Davis, A., In van de Waterbeemd, H. (Ed.), Adv. Comp.-Ass. Tech. Drug Discovery, VCH, New York, NY, 1994, pp. 39–60.
6. Cramer, R.D. III, Patterson, D. and Bunce, B., J. Am. Chem. Soc., 110 (1988) 5959.
7. Lindberg, W., Persson, J.A. and Wold, S., Anal. Chem., 55 (1983) 643.
8. Dunn, W.J., III, Wold, S., Edlund, U., Hellberg, S. and Gasteiger, J., Quant. Struct.Act. Relat. Pharmacol., Chem. Biol., 3 (1984) 131.
9. For a recent example of this approach see: Cho, S.J., Serrano G.M.L., Bier, J. and Tropsha, A., J. Med. Chem., 39 (1996) 5064.
10. Marshall, G.R., Barry, C.D., Bossghard, H.E., Dammkoehler, R.A. and Dun, D.A., In Olson, E.C. and Christoffersen, R.E. (Eds), Computer-Assisted Drug Design, ACS Symp. Series, Vol. 112, American Chemical Society, Washington, DC, 1979, 205–226.
11. Mayer, D., Naylor, C.B., Motoc, I. and Marshall, G.R., J. Comput.-Aided Mol. Design, 1 (1987) 3.
12. Dammkoehler, R.A., Karasek, S.F., Shands, E.F.B. and Marshall, G.R., J. Comput.-Aided Mol. Design, 3 (1989) 3.
13. For an example see: DePriest, S.A., Mayer, D., Naylor, C.B. and Marshall, G.R., J. Am. Chem. Soc., 115 (1993) 5372.
14. Martin, Y.C., Bures, M.G., Danaher, E.A, DeLazzer, J., Lico, I. and Pavelik, P.A., J. Comput.-Aided Mol. Design, 7 (1993) 83.
15. Myers, A.M., Charfison, P.S., Owens, C.E., Kula, N.S., McPhail, A.T., Baldessarini, R.J., Booth, R.G. and Wyrick, S.D., J. Med. Chem., 37 (1994) 4109.
16. Barnum, D., Greene, J., Smellie, A. and Sprague, P., J. Chem. Inf. Comput. Sci., 36 (1996) 563.
17. Smellie, A., Teig, S.L. and Towbin, P., J. Comput. Chem., 16 (1995) 171.
18. Langer, T. and Hoffman, R.D., J. Chem. Inf. Comput. Sci., 38 (1998) 325.
19. Bargar, T.M., Secor, J., Markley, L.D., Shaw, B.A. and Erickson, J.A., Pest. Sci., 55 (1999) 1059.
20. SYBYL, version 6.4, 1997, Tripos Inc, St. Louis, MO.
21. Clark, M., Cramer, R.D. III, Jones, D.M., Patterson, D.E. and Simeroth, P.E., Tet. Comput. Meth., 3 (1990) 47.
22. Rault, S., Bureau, R., Pilo, J.C. and Robba, M., J. Comput.-Aided Mol. Design, 6 (1992) 553.
23. Klebe, G. and Abraham, U., J. Med. Chem., 36 (1993) 70.
24. Kearsley, S.K. and Smith, G.M., Tet. Comput. Meth., 3 (1990) 615.
25. Horowitz, J.P., Massova, I., Wiese, T.E., Besler, B.H. and Corbett, T.H., J. Med. Chem., 37 (1994) 781.
26. Tafi, A., Anasttassopoulou, J., Theophanides, T., Botta, M., Corelli, F., Massa, S., Artico, M., Costi, R., Di Santo, R. and Rango, R., J. Med. Chem., 39 (1996) 1227.
27. Carrigan, S.W., Fox, P.C., Wall, M.E., Wan, M.C. and Bowen, J.P., J. Comput.-Aided Mol. Design, 11 (1997) 71.
28. Clark, R.D., Parlow, J.J., Brannigan, L.H., Schnur, D.M. and Duewer, D.L., In Hansch, C. and Fujita, T. (Eds), Classical and Three-Dimensional QSAR in Agrochemistry, ACS Symp. Series, Vol. 606, American Chemical Society, Washington, DC, 1995, pp. 264–281.
29. Folkers, G., Merz, A. and Rognan, D., In Wermuth, C.G. (Ed.), Trends in QSAR and Molecular Modeling 92, ESCOM, Leiden, 1993, pp. 233–244.
30. Ortiz, A.R., Pastor, M., Palomer, A., Cruciani, U., Gago, F. and Wade, R.C., J. Med. Chem., 40 (1997) 1136.
31. Waller, C.L., Oprea, T.I., Giolitti, A. and Marshall, G.R., J. Med. Chem., 36 (1993) 4152.
32. Oprea, T.I., Waller, C.L. and Marshall, G.R., J. Med. Chem., 37 (1994) 2206.
33. Schmetzer, S., Greenidge, P., Kovar, K.-A., Meike, S.-A. and Folkers, G., J. Comput.-Aided Mol. Design, 11 (1997) 278.
34. Vedani, A., Zbinden, P., Snyder, J.P. and Greenidge, P.A., J. Am. Chem. Soc., 117 (1995) 4987.
35. Zbinden, P., Dobler, M., Folkers, G. and Vedani, A., Quant. Struct.-Act. Relat., 17 (1998) 122.
36. Sanchez, R. and Sali, A., Curr. Opin. Struct. Biol., 7 (1997) 206.
37. Boehm, G., Biophys. Chem., 59 (1996) 1.
38. Johnson, M.S., Srinivasan, N., Sowdhamini, R. and Blundell, T.L., Crit. Rev. Biochem. Mol. Biol., 29 (1994) 1.
39. Ortiz, A.R., Pisabarro, M.T., Gago, F. and Wade, R.C., J. Med. Chem., 38 (1995) 2681.
40. Tokarski, J.S. and Hopfinger, A.J., J. Chem. Inf. Comput. Sci., 37 (1997) 779, 792.
41. Artico, M., Botta, M., Corelli, F., Mai, A., Massa, S. and Ragno, R., Bioorg. Med. Chem., 4 (1996) 1715.
42. Carrieri, A., Altomare, C., Barreca, M.L., Contento, A., Carotti, A. and Hansch, C., Il Farmaco, 49 (1994) 573.
43. Gainper, A.M., Winger, R.H., Liedl, K.R., Sotriffer, C.A., Varga, J.M., Kroemer, R.T. and Rode, B.M., J. Med. Chem., 39 (1996) 2882.
44. Goodsell, D.S. and Olsen, A.J., Proteins Struct. Funct. Genet., 8 (1990) 195.
45. Kuntz, I.D., Blaney, J.M., Oatley, S.J., Langridge, R. and Ferrin, T.E., J. Mol. Biol., 161 (1982) 269.
46. Shoichet, B.K., Bodian, D.L. and Kuntz, I.D., J. Comput. Chem., 13 (1992) 380.
47. Meng, E.C., Shoichet, B.K. and Kuntz, I.D., J. Comput. Chem., 13 (1992) 505.
48. Meng, E.C., Gschweng, D.A., Blaney, J.M. and Kuntz, I.D., Proteins Struct. Funct. Genet., 17 (1993) 266.
49. Leach, A.R. and Kuntz, I.D., J. Comput. Chem., 13 (1992) 730.
50. Ewing, T.J.A. and Kuntz, I.D., J. Comput. Chem., 18 (1997) 1175.
51. Bowyer, J., Hilton, M., Whitelegge, J., Jewess, P., Camilleri, P., Crofts, A. and Robinson, H., Z. Naturforsch., 45c (1990) 379.

52. Tietjen, K.G., Kluth, J.F., Anfree, R., Haug, M., Lindig, M., Muller, K.H., Wroblowsky, H.J. and Trebst, A., Pest. Sci., 31 (1991) 65.

53. Ruffle, S.V., Donnelly, D., Blundell, T.L. and Nugent, J.H.A., Photosynthesis Res., 34 (1992) 287.

54. Egner, U., Hoyer, G.-A. and Saenger, W., Eur. J. Biochem., 206 (1992) 685.

55. Egner, U., Hoyer, G.-A. and Saenger, W., Biochim. Biophys. Acta, 1142 (1993) 106.

56. Mackay, S.P. and O'Malley, P.J., Z. Naturforsch., 48c (1993), 773.

57. Sobolev, V. and Edelman M., Proteins Struct. Funct. Genet., 21 (1995) 214.

58. Svensson, B., Etchebest, C., Tuffery, P., van Kan, P., Smith, J. and Styring, S., Biochemistry, 35 (1996) 14486.

59. Egner, U., Gerbling, K.P., Hoyer, G.-A., Kruger, G. and Wegner, P., Pest. Sci., 47 (1996) 145.

60. Deisenhofer, J., Epp, O., Miki, K., Huber, R. and Michel, H., Nature, 318 (1985) 618.

61. Michel, H. and Deisenhofer, J., Biochemistry, 27 (1988) 1.

62. Draber, W., Tietjen, K., Kluth, J.F. and Trebst, A., Angew. Chem. Int. Ed. Engl., 30 (1991) 1621.

63. Huppazt, J.L., Weed Sci., 44 (1996) 743.

64. Vaz, R., Weed Sci., 44 (1996) 718.

65. Draber, W., Trebst, A. and Oettmeier, W., In Hansch, C. and Fujita, T. (Eds), Classical and Three-Dimensional QSAR in Agrochemistry, ACS Symp. Series, Vol. 606, American Chemical Society, Washington, DC, 1995, pp. 186–198.

66. Eilers, R.J., Crouse, G.D., Durst, G.L., Manly, C.J., Webster, J.D. and Streusand, V.J., Pest. Biochem. Phys., 43 (1992) 162.

67. QUANTA, 1997, Molecular Simulations Inc., San Diego, CA.

68. Zurawksi, G., Bohnert, H.J., Whitfeld, P.R. and Bottomley, W., Proc. Natl. Acad. Sci. USA, 79 (1982) 7699.

69. CHARMm, 1997, Molecular Simulations Inc., San Diego, CA.

70. Brooks, B.R., Bruccoleri. R.E., Olafson, B.D., States, D.J., Swaminathan, S. and Karplus, M., J. Comput. Chem., 4 (1983) 187.

71. DOCK version 4.0, University of California, 1997, San Fransisco, CA.

72. CONCORD 4.0, 1998, University of Texas, Austin, TX.

73. Gasteiger, J. and Marsili, M., Tetrahedron, 36 (1980) 3219.

74. Marsili, M. and Gasteiger, J., Croat. Chem. Acta, 53 (1980) 601.

75. Cho, S.J. and Tropsha, A., J. Med. Chem., 38 (1995) 1060.

76. Sulea, T., Oprea, T.I., Muresan, S. and Chan, S.L., J. Chem. Inf. Comput. Sci., 3 (1997) 1162.

77. Bush, B.L. and Nachbar, R.B., J. Comput.-Aided Mol. Design, 7 (1993) 587.

78. Lindgren, F., Geladi, P., Ranner, S. and Wold, S., J. Chemometrics, 8 (1994) 349.

79. Verloop, A., Hoogenstraaten, W. and Tipker, J., Med. Chem., 11 (1976) 165.